JOURNAL OF APPLIED PHYSICS VOLUME 90, NUMBER 3 1 AUGUST 2001

# Image charge forces inside conducting boundaries

Mark D. Tinkle[a] and S. E. Barlow[b]
*W. R. Wiley Environmental Molecular Sciences Lab, Pacific Northwest National Laboratory,*
*P.O. Box 999 (K8-88), Richland, Washington 99352*

(Received 7 June 2000; accepted for publication 3 May 2001)

The common description of the electrostatic force, $\mathbf{F}(\mathbf{x}) = -q\nabla\phi(\mathbf{x})$, provides an incomplete description of the force on the charge $q$ at a point $\mathbf{x}$ when the charge itself induces additional fields, e.g., image charges, polarizations, etc. The equation may be corrected through the introduction of a "pseudopotential" formalism. Exploration of some of the elementary properties of the pseudopotential demonstrates its essential simplicity. This simplicity allows it to be incorporated directly into dynamics calculations. We explicitly evaluate the pseudopotential in a number of simple but important cases including the sphere, parallel plates, the rectangular prism, and the cylindrical box. The pseudopotential formalism may be expanded to include extended charge distributions; in this latter form we are able to directly apply the results to experimental measurements. © *2001 American Institute of Physics.* [DOI: 10.1063/1.1383016]

## I. INTRODUCTION

The force on a charged particle due to the charges it induces on nearby conducting surfaces is a factor in many scientific measurements,[1–7] The effects of these forces are particularly important where high precision is sought;[4] conducting surfaces are very close;[5] a great deal of charge is used;[2] or a region is otherwise field free.[7] It has been recognized for some time that measurements of ion mass-to-charge ratios made in Penning trap based mass spectrometers can be affected by induced surface charges.[1,4,6] Until now, general techniques for quantifying image charge effects in these instruments have not been available. An earlier attempt to treat the cylinder problem was made by Xiang *et al.*,[8] but a subtle math error rendered their results incorrect, as we describe below. An important advance was made in a recent article by Fine and Driscoll[7] which addressed the lowest order solutions to this problem for infinite cylindrical geometry, including finite charge length effects. Here, we generalize those results considerably. We find that the standard description of electrostatic force given in most texts, i.e., $\mathbf{F}(\mathbf{x}) = -q\nabla\phi(\mathbf{x})$ is inadequate when image charge effects are included.

In the sections below, we present calculations of image charge forces for charges inside closed and infinitely extended geometries: the parallel plate, the sphere, the rectangular box, and the cylindrical box; the latter two geometries are widely employed in ion cyclotron resonance mass spectrometer (ICR) cells. Recently, cylindrical trap designs have also become popular for precision measurements.[9,10] This advance has reduced the need for detailed treatment of hyperboloidal trap geometries, without compromising the quality of the electrostatic trapping fields.[11] The classical hyperbolic trap electrode geometry requires a careful numerical treatment and lies outside the scope of this article.

We begin our development in Sec. II by reviewing some of the more important definitions and restrictions of our treatment. We then move on to demonstrate the inadequacy of the usual electric force equation and show that the deficiency can be remedied through the introduction of a "pseudopotential." Once found, the pseudopotential can then be used just like any other for determining forces and acceleration. Section II continues with a review of various techniques for treating image charge.

Our results are presented in Sec. III. We start with a generic limiting form to which all subsequent analysis can be referred. Consideration of the familiar spherical shell and parallel plate problems shows that both of these problems can readily be cast in terms of our generic form. In the last two parts of Sec. III we treat rectangular and cylindrical boxes. The derivations are rather lengthy and require the use of Green's functions. However, when the solutions are cast into the generic form, we once again find surprisingly simple behavior.

Understanding the effects of image charge in Penning trap mass spectrometers, particularly in ICRs is a major motivation for this work. In Sec. IV we show how image charge affects the $\mathbf{E}\times\mathbf{B}$ motion in these environments. In Sec. IV B, we show how our results can be extended to ion clouds of finite dimension. The results of this development are then applied to drift mode data from our own ICR instrument. Although the drift mode is well known to the broad ICR community, its importance is not widely appreciated. Many effects that reduce data quality have their origin in the drift mode. This is a point that we return to at the end of Sec. IV.

## II. DEFINITIONS AND METHODS

The term "image charge" is itself a misnomer, and this can be confusing. The term comes from the "method of images" which is but one, albeit powerful, technique for solving the general class of problems associated with the interaction of charges and conductors.[12] Physically, when a charge or charged body approaches a conductor held at some potential, say $\mathbf{V}$, charge flows from the potential source to

---

[a] Current address: Dynamics Technology, Inc., 21311 Hawthorne Blvd., Suite 300, Torrance, CA 90503-5610.

[b] Author to whom correspondence should be addressed; electronic mail: se.barlow@pnl.gov

the conductor. This charge arranges itself on the surface of the conductor in just such a way that the conductor's potential everywhere returns to **V** as required by Gauss's law. The surface charge distribution $\sigma$ gives rise to an additional field at the source particle that affects its motion. "Induced Charge Distribution" would probably be a better term, but as in so many other cases historical naming seems likely to prevail into the future. Since the location of the charged particle determines the surface charge distribution, many otherwise general techniques for finding solutions of Laplace's equation cannot be used because one cannot subtract the particle's Coulomb potential in any convenient way.

We are focussing on the effects on the real charge produced by its own image. Effects of the image charge on other charges can be found directly from the Green's function and are not considered further. Also, we are concerned here only with the nonrelativistic limit, i.e., we assume that all velocities are small compared to the speed of light and that all wavelengths are large compared to the scale lengths of the experimental apparatus. Relativistic effects have been discussed by Brown and Gabrielse[13] and Dehmelt *et al.*[14] Last, energy and distance scales that require quantum mechanical treatment also lie outside our scope here.

The calculation of potentials and forces on charges in the presence of conductors is addressed in various ways in the numerous texts on electrostatics, but no text that we are aware of presents a convenient summary of the available techniques. Further difficulties arise in applying any one of these techniques to the range of problems we wish to address. We have found it easiest to use different methods for different parts of our calculations. In this section we explain the techniques we will use.

### A. Image charge pseudopotential

The measurable physical variable associated with induced surface charge is the force it produces on the point charge. We would like to express this force as the gradient of a function of the point charge's position. There is a subtlety involved in this potential function that is best illustrated by a simple example using the method of images.

#### 1. Motivating example

If a point charge of strength $q$ is at a position $(x,y,z) = (x_0,0,0)$, $(x_0>0)$ with a grounded conductor in the $y-z$ plane, we know from the method of images[15] that the electrostatic potential for $x>0$ can be expressed as the sum of the potentials from the point charge and a fictitious image charge of strength $-q$ located at $(x,y,z)=(-x_0,0,0)$

$$\phi(x,y,z)=\frac{q}{4\pi\epsilon_0}\left(\frac{1}{\sqrt{[(x-x_0)^2+y^2+z^2)]}} - \frac{1}{\sqrt{[(x+x_0)^2+y^2+z^2)]}}\right) \tag{1}$$

for $x>0$. This is the potential that determines the force on an infinitesimal point charge, which is to say a point charge whose own induced surface charges produce negligible forces. Can we use it to find the force on the charge $q$? We must first drop the potential produced by the charge, since it cannot exert a force on itself. This leaves the potential of the image charge, which evaluated along the $x$ axis is just

$$\Phi_I(x,0,0)=\frac{-q}{4\pi\epsilon_0}\frac{1}{x+x_0} \tag{2}$$

for $x>0$. Two courses of action present themselves for finding the $x$ component of the force: take $\partial\Phi_I/\partial x$ and evaluate at $x=x_0$, or evaluate $\Phi_I$ at $x=x_0$ and take $\partial/\partial x_0$ of the result. The results differ by a factor of two

$$\left.\frac{\partial\Phi_I}{\partial x}\right|_{x=x_0}=\frac{q}{4\pi\epsilon_0}\frac{1}{4x_0^2}, \tag{3}$$

and

$$\frac{\partial[\Phi_I|_{x=x_0}]}{\partial x_0}=\frac{q}{4\pi\epsilon_0}\frac{1}{2x_0^2}. \tag{4}$$

The force can be found directly from Coulomb's Law using the image charge[15]

$$\mathbf{F}=\frac{-q^2}{4\pi\epsilon_0}\frac{1}{4x_0^2}\hat{x}, \tag{5}$$

so at least in this case, we have a choice of formulas for the force in terms of the potential

$$\mathbf{F}(x_0)=-q\left.\frac{\partial\Phi_I}{\partial x}\right|_{x=x_0}\hat{x} \tag{6}$$

or

$$\mathbf{F}(x_0)=\frac{-q}{2}\frac{\partial[\Phi_I|_{x=x_0}]}{\partial x_0}\hat{x}. \tag{7}$$

The first choice seems like the natural one, but it requires us to keep a function of two position coordinates ($x$ and $x_0$). The second choice contains an unfamiliar factor of 1/2, but the force is reconstructed from a simple function of one position coordinate ($x_0$). This is the useful form, which we will now derive more generally.

#### 2. General derivation

Motivated by this example, we will show that a general expression for the force on a point charge $q$ in the presence of both fixed charges and conductors at fixed potentials is

$$\mathbf{F}=-q\nabla\phi-\tfrac{1}{2}q\nabla\Phi, \tag{8}$$

where $\phi$ is the ordinary electrostatic potential due to the fixed charges and potentials, and $\Phi$ is the image charge pseudopotential, the potential due to charges induced by the point charge, evaluated at the point charge coordinate.

From the definition of the electrostatic potential $\phi$, the work required to bring a point charge $q$ in to position $\mathbf{x}$ from infinity (where $\phi=0$) while holding the charges producing $\phi$ fixed in place is $W=q\phi(\mathbf{x})$. The force on the particle is the negative of the gradient with respect to its position coordinate of the *total system energy* under the circumstances considered. If the charges producing $\phi(\mathbf{x})$ are indeed fixed and there are no other energy terms involving the position of the point charge, then the force is $\mathbf{F}=-q\nabla\phi$. This is the familiar result for an infinitesimal test charge, but it is a special case. It is not the definition of $\phi$.

When a charge moves toward a conducting surface, the induced surface charges must bunch together, against their mutual repulsion, to maintain an equipotential. This adds a term to the total electrostatic energy of the system that acts to reduce the attractive force felt by the point charge, by exactly a factor of two. This is easily derived from the well-known expression for the total electrostatic energy (excluding self-energy) of $n$ discrete charges

$$W=\frac{1}{2}\sum_{j=1}^{n} q_j\Phi_j\,, \tag{9}$$

where $\Phi_j$ is the potential at charge $q_j$ due to all the other charges.[14] If $j=1$ denotes the point charge, and the others are the charges induced on a grounded conductor, then $\Phi_j$ is zero for all $j\neq 1$ (the induced charges) regardless of the position of the point charge, and the total electrostatic energy is

$$W=\tfrac{1}{2}q\Phi, \tag{10}$$

where $\Phi=\Phi_1$ is the potential at the point charge due to the induced surface charges. The force on the point charge is thus

$$\mathbf{F}=-\tfrac{1}{2}q\nabla\Phi, \tag{11}$$

where the gradient is taken with respect to the position of the point charge. If the conductor is at some potential other than ground, then we must add the familiar term $-q\nabla\phi$ to this thereby recovering Eq. (8).

We refer to $\Phi(\mathbf{x})$ as the image charge pseudopotential, to emphasize its differences from ordinary potentials. Unlike $\phi(\mathbf{x})$, $\Phi(\mathbf{x})$ is not simply a solution of Laplace's or Poisson's equation, because its source term (the induced charge distribution) is a complicated functional of $\mathbf{x}$, the point charge location. Further, $\Phi(\mathbf{x})$ is only meaningful at the particular location of the charge. As we describe below, $\Phi(\mathbf{x})$ is proportional to the nonsingular part of $G(\mathbf{x},\mathbf{x}')$, evaluated at $\mathbf{x}=\mathbf{x}'$. Thus, $\Phi(\mathbf{x})$ may be extracted from a family of solutions to Laplace's equation, but is not itself a solution.

### B. Method of images

In cases where the classical method of images can be applied, as in the preceding example, the force can be found directly from Coulomb's law, treating the discrete image charges as real. The pseudopotential can be found in the same way. In Secs. III B and III C, we use the method of images to find $\Phi$ for a point charge inside a spherical conducting shell and for a point charge between infinite parallel conducting plates. The example of a point charge near a single infinite plate will be shown to be a limiting form near any smooth surface.

### C. Green's function techniques

The electrostatic Green's function $G(\mathbf{x},\mathbf{x}')$ is the potential that an infinitesimal test charge would feel at $\mathbf{x}$ due to a unit point charge at $\mathbf{x}'$, in the presence of grounded conductors of a specified geometry. Clearly $G$ contains $\Phi$, and a great deal more. If the method of images can be applied to a problem, then a simple Green's function can also be found and will give the same results. More generally, determining the Green's function is difficult or impossible, but for cylinders and rectangular boxes infinite series expansions for $G$ in various different forms are known, and we will use them to find $\Phi$ for these geometries.

#### 1. Evaluation of *G* at $\mathbf{x}=\mathbf{x}'$

The Green's function can be written as

$$G(\mathbf{x},\mathbf{x}')=\frac{1}{4\pi\epsilon_0|\mathbf{x}-\mathbf{x}'|}+H(\mathbf{x},\mathbf{x}'), \tag{12}$$

where $H$ is the contribution from the induced surface charges, so $\Phi(\mathbf{x})=qH(\mathbf{x},\mathbf{x})$. In simple cases amenable to solution by the method of images, $G$ will clearly separate into these pieces, but unfortunately this is not true of the infinite series forms for $G$ for cylinders and boxes. One straightforward solution is to use a computer to estimate $\Phi$ from the limit as $\mathbf{x}$ approaches $\mathbf{x}'$:

$$\Phi(\mathbf{x})=q\lim_{\mathbf{x}\to\mathbf{x}'}\left(G(\mathbf{x},\mathbf{x}')-\frac{1}{4\pi\epsilon_0|\mathbf{x}-\mathbf{x}'|}\right). \tag{13}$$

#### 2. Direct evaluation of *H*$(\mathbf{x},\mathbf{x}')$

In some cases, the function $H(\mathbf{x},\mathbf{x}')$ is known or can be found explicitly, and allows the direct evaluation of $\Phi(\mathbf{x})$. This technique was employed by Fine and Driscoll[7] for the infinite cylinder geometry. They showed how to reduce the well-known solution of an infinitely long charged column in an infinite cylinder (see Davidson,[3] Sec. 5.4) to a finite one and finally to a single point charge. We do not use this approach here, but it does provide a useful check.

#### 3. Gradient of *G*

Following Smythe,[12] the force on the charge can be found by evaluating $G$ at $\mathbf{x}'=\mathbf{x}$ and taking the gradient

$$\mathbf{F}=-q^2\nabla G(\mathbf{x},\mathbf{x})/2, \tag{14}$$

the idea being that the self-field term must vanish, since it cannot result in a force on the charge. (Note how the factor of one half appears here.) This is a rather problematic equation, since $G$ is evaluated at its pole, and it can only be considered shorthand for a more proper limiting procedure. Still, since the individual terms of the series expressions for $G$ for cylinders and boxes are finite at $\mathbf{x}=\mathbf{x}'$, the equation may be naively applied term by term. There is no reason to expect that the resulting series expression for $\mathbf{F}$ will converge, but it often does.

#### 4. Force on the conductors

The charge distribution $\sigma$ on a surface $S$ can be found from the Green's function as follows:

$$\sigma=-\epsilon_0 q\nabla G(\mathbf{x},\mathbf{x}')\cdot d\mathbf{a}\big|_{\mathbf{x}\in S}\,, \tag{15}$$

where the gradient is taken with respect to $\mathbf{x}$. The force on the point charge due to $\sigma$ can be calculated from Coulomb's law, but it is easier to find the total force on the conductors, which from Newton's third law is the negative of the force on the charge.[15] The surface charge creates a pressure

$$p = \sigma^2 / 2\epsilon_0, \tag{16}$$

directed out of the conductor. The force on the charge is thus

$$\mathbf{F} = -\int_S \sigma^2 da / 2\epsilon_0. \tag{17}$$

This is the technique used by Xiang *et al.*[8]

### D. Numerical computation

If the Green's function is not known, useful results can be obtained from numerical solutions to Laplace's equation. From Eq. (12) it is clear that $H(\mathbf{x},\mathbf{x}')$ is a solution to Laplace's equation that satisfies the unusual boundary condition

$$H(\mathbf{x},\mathbf{x}') = -\frac{1}{4\pi\epsilon_0 |\mathbf{x}-\mathbf{x}'|} \tag{18}$$

for $\mathbf{x} \in S$. Computation of $H(\mathbf{x},\mathbf{x}')$ for a particular value of $\mathbf{x}'$ yields the pseudopotential at that point

$$\Phi(\mathbf{x}') = qH(\mathbf{x}',\mathbf{x}'). \tag{19}$$

This technique can be used, for instance, to study hyperboloidal geometries, but as stated above, lies outside the scope of the present treatment.

## III. RESULTS

### A. Generic limiting form

As a smooth region of a conductor is approached closely, the pseudopotential approaches that of an infinite flat plate. From the method of images, $\Phi \rightarrow -q/4\pi\epsilon_0 2d$ as $d \rightarrow 0$, where $d$ is the distance to the surface. Thus if $\xi_0$ is the distance to a conductor along the $\xi$ axis of a rectilinear coordinate system and the surface is perpendicular to the $\xi$ axis where they intersect,

$$\Phi \rightarrow -\frac{q}{4\pi\epsilon_0 \xi_0} \frac{1}{2(1-\overline{\xi})}, \tag{20}$$

as $\overline{\xi} \equiv \xi/\xi_0 \rightarrow 1$. If the geometry is symmetric in $\xi$, we can account for the limiting behaviors at both walls with the form

$$\Phi \rightarrow -\frac{q}{4\pi\epsilon_0 \xi_0} \frac{1}{1-\overline{\xi}^2} \tag{21}$$

as $\overline{\xi} \rightarrow \pm 1$. The complete solution for $\Phi$ along the $\xi$ axis will be the sum of this divergent term and a finite term. Expressed as a power series expansion about the origin, it will have the form

$$\Phi = -\frac{q}{4\pi\epsilon_0 \xi_0} \sum_{n=0}^{\infty} C_n \overline{\xi}^n, \tag{22}$$

with $C_n = 0$ for odd $n$, due to symmetry. The divergent term by itself has $C_n = 1$ for all even $n$. The results we obtain for specific geometries can all be expressed in this form, with different values for the coefficients.

### B. Spherical shell

A single image charge can be used to represent the potential inside a spherical conducting shell of radius $r_0$ due to surface charges[15] induced by a point charge $q$ at a radius $r < r_0$. The image charge lies along the same ray from the origin as the point charge, at a radius $r' = r_0^2/r$, and has charge $q' = -qr_0/r$. The pseudopotential can be written as

$$\Phi = -\frac{q}{4\pi\epsilon_0 r_0} \frac{1}{1-\overline{r}^2}, \tag{23}$$

where $\overline{r} \equiv r/r_0$. For small displacements from the center of the sphere, it is useful to express $\Phi$ as a power series in $\overline{r}$

$$\Phi = -\frac{q}{4\pi\epsilon_0 r_0} (1 + \overline{r}^2 + \overline{r}^4 + \overline{r}^6 + \cdots). \tag{24}$$

Note that this result, which is exact, is identical to the limiting form obtained in the previous section.

### C. Parallel plates

The pseudopotential of a charge $q$ between two infinite grounded parallel plates can be found by the method of images. This provides a useful check for the more difficult cylinder and rectangular box calculations, of which it is a limiting case. Let the plates be parallel to the $xy$ plane and located at $z = \pm z_0$. If the charge has $z$-coordinate $z'$, an image charge $-q$ at $z = 2z_0 - z'$ will produce the required boundary condition at the $z = z_0$ plate, and another charge $-q$ at $z = -2z_0 - z'$ is needed for the other plate. Unfortunately, each of these image charges affects the potential at the other plate and must be countered by its own image charge, producing an infinite sequence of image charges, all of the same magnitude, but with alternating sign. The $-q$ image charges are spaced evenly along the $z$ axis, separated by $4z_0$. The $q$ image charges are also evenly spaced with separation $4z_0$, with one missing from the pattern at $z = z'$. The potential at $z'$ due to all these image charges is, after some rearrangement

$$\Phi = -\frac{q}{4\pi\epsilon_0 z_0} \left\{ \ln(2) + \sum_{j=1}^{\infty} \frac{z^2}{(2j-1)[(2j-1)^2 z_0^2 - z^2]} \right\}, \tag{25}$$

where we have now substituted $z$ for $z'$. The terms of the series can be regrouped as

$$\Phi = -\frac{q}{4\pi\epsilon_0 z_0} \sum_{m=1}^{\infty} C_{2m} \left( \frac{z}{z_0} \right)^{2m}, \tag{26}$$

where

$$C_{2m} = \sum_{j=0}^{\infty} \frac{1}{(2j+1)^{2m+1}}, \quad m > 0. \tag{27}$$

Evaluating the first few terms, we find: $C_0 = \ln(2)$, $C_2 \approx 1.0518$, $C_4 \approx 1.0045$, and $C_6 \approx 1.0005$. Again, this is very close to the generic form, with the biggest differences found in the lowest order terms of the expansion. In the more complex cases of rectangular and cylindrical boxes considered below, these values represent limiting cases and can be used to verify the correctness of our derivations. (This is the last case we consider where $C_0$ is determined.)

### D. Rectangular box

Now consider a rectangular box with boundaries at $x = \pm x_0$, $y = \pm y_0$, and $z = \pm z_0$. The mathematical notation is simplified by scaling the coordinates by these dimensions, i.e., $\tilde{x} = x/x_0$, $\tilde{y} = y/y_0$ and $\tilde{z} = z/z_0$. The shape can be described by two "aspect ratios," $\alpha = z_0/x_0$ and $\beta = z_0/y_0$. One form for the Green's function of the interior of the box is

$$G(\tilde{x},\tilde{y},\tilde{z}) = \frac{z_0}{\epsilon_0 x_0 y_0} \times \sum_{l=1}^{\infty} \sum_{m=1}^{\infty} \frac{\sinh[k_{lm}(1+\tilde{z}_<)]\sinh[k_{lm}(1-\tilde{z}_>)]}{k_{lm}\sinh(2k_{lm})} \times \left\{ \sin\left[\frac{l\pi}{2}(\tilde{x}+1)\right] \sin\left[\frac{l\pi}{2}(\tilde{x}'+1)\right] \times \sin\left[\frac{m\pi}{2}(\tilde{y}+1)\right] \sin\left[\frac{m\pi}{2}(\tilde{y}'+1)\right] \right\}, \tag{28}$$

where

$$k_{lm} = \frac{\pi z_0}{2}\left(\frac{l^2}{x_0^2} + \frac{m^2}{y_0^2}\right)^{1/2}. \tag{29}$$

The coordinate $\tilde{z}_<$ is the lesser of $\tilde{z}$ and $\tilde{z}'$, and $\tilde{z}_>$ is the greater. The coordinates in Eq. (28) can of course be permuted at will. The image forces can be readily evaluated using Eq. (14). This is particularly true for the $z$ axis, where the sinh functions assure rapid numerical convergence except very near the walls. Having once found $F_z$, forces in the orthogonal directions, $x$ and $y$ can be written down immediately simply by permuting the variables. We find

$$F_z = \frac{q^2}{2\epsilon_0 x_0 y_0} \sum_{l=1}^{\infty} \sum_{m=1}^{\infty} \left\{ \sin\left[\frac{l\pi}{2}(\tilde{x}+1)\right]\right\}^2 \times \left\{ \sin\left[\frac{m\pi}{2}(\tilde{y}+1)\right]\right\}^2 \frac{\sinh[2k_{lm}\tilde{z}]}{\sinh(2k_{lm})}. \tag{30}$$

Equation (30) can be integrated to give the parts of the pseudopotential that contain all terms of the forms: $z^n, x^m z^n, y^p z^n$, and $x^m y^p z^n$. Only terms of the form $x^m, x^m y^p$, and $y^p$ remain. Using the above definitions for $\alpha$ and $\beta$, we rewrite $k_{lm}$ and define two new functions, $g_{lm}$ and $h_{lm}$

$$k_{lm} = \frac{\pi}{2}\sqrt{\alpha^2 l^2 + \beta^2 m^2}, \tag{31}$$

$$g_{lm} = \frac{\pi}{2\beta}\sqrt{\alpha^2 l^2 + (2m-1)^2}, \tag{32}$$

and

$$h_{lm} = \frac{\pi}{2\alpha}\sqrt{\beta^2(2l-1)^2 + (2m-1)^2}. \tag{33}$$

We can then write the image charge pseudopotential explicitly as

$$\Phi(\tilde{x},\tilde{y},\tilde{z}) = -\frac{q}{2\epsilon_0 z_0}\alpha\beta \left\{ \sum_{l=1}^{\infty}\sum_{m=1}^{\infty} \frac{\left[\sin\left(\frac{l\pi}{2}\{1+\tilde{x}\}\right)\right]^2 \left[\sin\left(\frac{m\pi}{2}\{1+\tilde{y}\}\right)\right]^2 [\cosh(2k_{lm}\tilde{z})-1]}{k_{lm}\sinh((2k_{lm}))} + \sum_{l=1}^{\infty}\sum_{m=1}^{\infty} \frac{\left[\sin\left(\frac{l\pi}{2}\{1+\tilde{x}\}\right)\right]^2 [\cosh(2g_{lm}\tilde{y})-1]}{\beta g_{lm}\sinh((2g_{lm}))} + \sum_{l=1}^{\infty}\sum_{m=1}^{\infty} \frac{[\cosh(2h_{lm}\tilde{x})-1]}{\alpha h_{lm}\sinh[(2h_{lm})]} \right\}, \tag{34}$$

neglecting an additive constant. The three components on the right hand side of Eq. (34) may be identified as those containing all of the $z$ terms, the remaining $y$ terms and the pure $x$ respectively. Equation (34) may be used directly to evaluate all of the image charge electric fields on a particle in a rectangular box, however, except for the "$z$" terms convergence is relatively poor. We find better performance by simply using the first term and permuting the variables while keeping the definitions of $\alpha$ and $\beta$. Following our general approach, each term in the sums can be expanded in a Taylor series and rearranged to get

$$\Phi(\tilde{x},\tilde{y},\tilde{z}) = -\frac{q}{4\pi\epsilon_0 z_0}\sum_{t=0}^{\infty}\sum_{u=0}^{\infty}\sum_{s=0}^{\infty} C_{2t,2u,2s}(\alpha,\beta)\tilde{x}^{2t}\tilde{y}^{2u}\tilde{z}^{2s}, \tag{35}$$

$s = t = u = 0$, is excluded.

By symmetry only even powers of the coordinates survive. In the sample calculations below, we consider the square prism, where $\alpha = \beta$. We will give explicit forms for the C's in this case. Note that since Eq. (34) does not give the constant term, we cannot find $C_{0,0,0}$ from the methods here.

### 1. The square prism

The effects of image charge on a particle in a square prism can be directly applied to observations made in standard ICR cells. For the square prism, $\alpha=\beta$ and the equations simplify somewhat. We define $D_0=x_0=y_0$ so that $z_0 = \alpha D_0$. We can now use Eq. (34) to evaluate the C's by expanding the various functions in power series. The results may be summarized as

$$C_{0,0,2s}(\alpha)=4\,\frac{\pi^{2s}\alpha^{2s+1}}{(2s)!}\sum_{l=1}^{\infty}\sum_{m=1}^{\infty}\frac{([2m-1]^2+[2l-1]^2)^{s-(1/2)}}{\sinh(\pi\sqrt{[2m-1]^2+[2l-1]^2}\,\alpha)}, \tag{36}$$

$$C_{2s,0,0}(\alpha)=C_{0,2s,0}(\alpha)=C_{0,0,2s}(\alpha^{-1}), \tag{37}$$

$$C_{2s,2t,0}(\alpha)=2\,\frac{\pi^{2s+2t}\alpha^{-2s}}{(2s)!(2t)!}\sum_{l=1}^{\infty}\sum_{m=1}^{\infty}\frac{([2m-1]^2+l^2\alpha^2)^{s-(1/2)}(-1)^{l+t}l^{2t}}{\sinh\left(\dfrac{\pi\sqrt{(2m-1)^2+l^2\alpha^2}}{\alpha}\right)}, \tag{38}$$

$$\left.\begin{matrix}C_{2t,0,2s}(\alpha)\\ C_{0,2t,2s}(\alpha)\end{matrix}\right\}=2\,\frac{(-1)^t\pi^{2s+2t}\alpha^{2s+1}}{(2s)!(2t)!}\sum_{l=1}^{\infty}\sum_{m=1}^{\infty}\frac{(-1)^l([2m-1]^2+l^2)^{s-(1/2)}l^{2t}}{\sinh(\pi\sqrt{[2m-1]^2+l^2}\,\alpha)}, \tag{39}$$

and

$$C_{2t,2u,2s}(\alpha)=\frac{(-1)^{t+u+1}\pi^{2s+2t+2u}\alpha^{2s+2t+2u+1}}{(2s)!(2t)!(2u)!}\sum_{l=1}^{\infty}\sum_{m=1}^{\infty}\frac{(-1)^{m+l}(m^2+l^2)^{s-(1/2)}m^{2u}l^{2t}}{\sinh(\pi\sqrt{m^2+l^2}\,\alpha)}. \tag{40}$$

We are now in a position to explore the consequences of varying the trap lengths. Figure 1 shows plots for the low order terms of Eqs. (36)–(40). Based on the discussion above on simpler systems, the qualitative, asymptotic behavior of these equations is as expected. Namely, as $\alpha\to 0$, the system becomes like the parallel plate case, with the pure $z$ terms converging near unity and all of the rest going to zero. In a similar vein, as $\alpha\to\infty$, the axial terms disappear and the transverse terms tend toward constant values. Table I lists the asymptotic limits of the C's from the figures. It is interesting to note that many of the nonlinear terms have maxima in the vicinity of $\alpha=1$, the cubic box, which is close to the aspect ratio most commonly employed in ICR work.

## E. Cylindrical shell

In comparison to the rectangular box, the calculations for a cylindrical box (including the infinitely long one) present greater difficulties. We note that the following mathematics are rather complicated; however, in the end we find that the expressions for $\Phi$ in powers of $r$ and $z$ are readily understood.

One expression for the Green's function of the interior of a cylinder of radius $\rho_0$ and length $2z_0$ is

$$G(\overline{\rho},\phi,\overline{z},\overline{\rho'},\phi',\overline{z'})$$

$$=\frac{1}{\pi\epsilon_0\rho_0}\sum_{m=0}^{\infty}\sum_{n=1}^{\infty}\left\{\frac{\epsilon_m\cos[m(\phi-\phi')]J_m(j_{m,n}\overline{\rho})J_m(j_{m,n}\overline{\rho'})}{j_{m,n}J_{m+1}^2(j_{m,n})}\,\frac{\sinh[j_{m,n}(\alpha+\overline{z_<})]\sinh[j_{m,n}(\alpha-\overline{z_>})]}{\sinh(2j_{m,n}\alpha)}\right\}, \tag{41}$$

where $\epsilon_m=2-\delta_{m,0}$; $\delta_{0,0}=1$, and $\delta_{m,0}=0$ otherwise; $j_{m,n}$ is the $n$th zero of the Bessel function $J_m(x)$; and $\alpha=z_0/\rho_0$ is the "aspect ratio" of the cylinder. The $\rho$ and $z$ coordinates are scaled by $\rho_0$ and their origin is the center of the cylinder. The coordinate $z_<$ is the lesser of $z$ and $z'$, and $z_>$ is the greater. The $z$ component of the force on a charge $q$ can be found by applying[12] Eq. (14) to $G$

$$F_z=\frac{q^2}{2\pi\epsilon_0\rho_0^2}\sum_{m=0}^{\infty}\sum_{n=1}^{\infty}\epsilon_m\frac{J_m^2(j_{m,n}\overline{\rho})}{J_{m+1}^2(j_{m,n})}\,\frac{\sinh(2j_{m,n}\overline{z})}{\sinh(2j_{m,n}\alpha)}. \tag{42}$$

The same approach for the radial force yields a divergent series, as mentioned above. Instead we find the force on the conductor using Eq. (17). Since the radial force is produced entirely by charges induced on the cylindrical wall, it is easier to use an alternate form for the Green's function

$$G(\tilde{\rho},\phi,\tilde{z},\tilde{\rho}',\phi',\tilde{z}')$$

$$=\frac{1}{2\pi\epsilon_0 z_0}\sum_{m=0}^{\infty}\sum_{n=1}^{\infty}\left\{\epsilon_m\cos[m(\phi-\phi')]\sin\left[\frac{n\pi(\tilde{z}+1)}{2}\right]\right.$$

$$\left.\times\sin\left[\frac{n\pi(\tilde{z}'+1)}{2}\right]T_n(\tilde{\rho},\tilde{\rho}')\right\}, \tag{43}$$

where

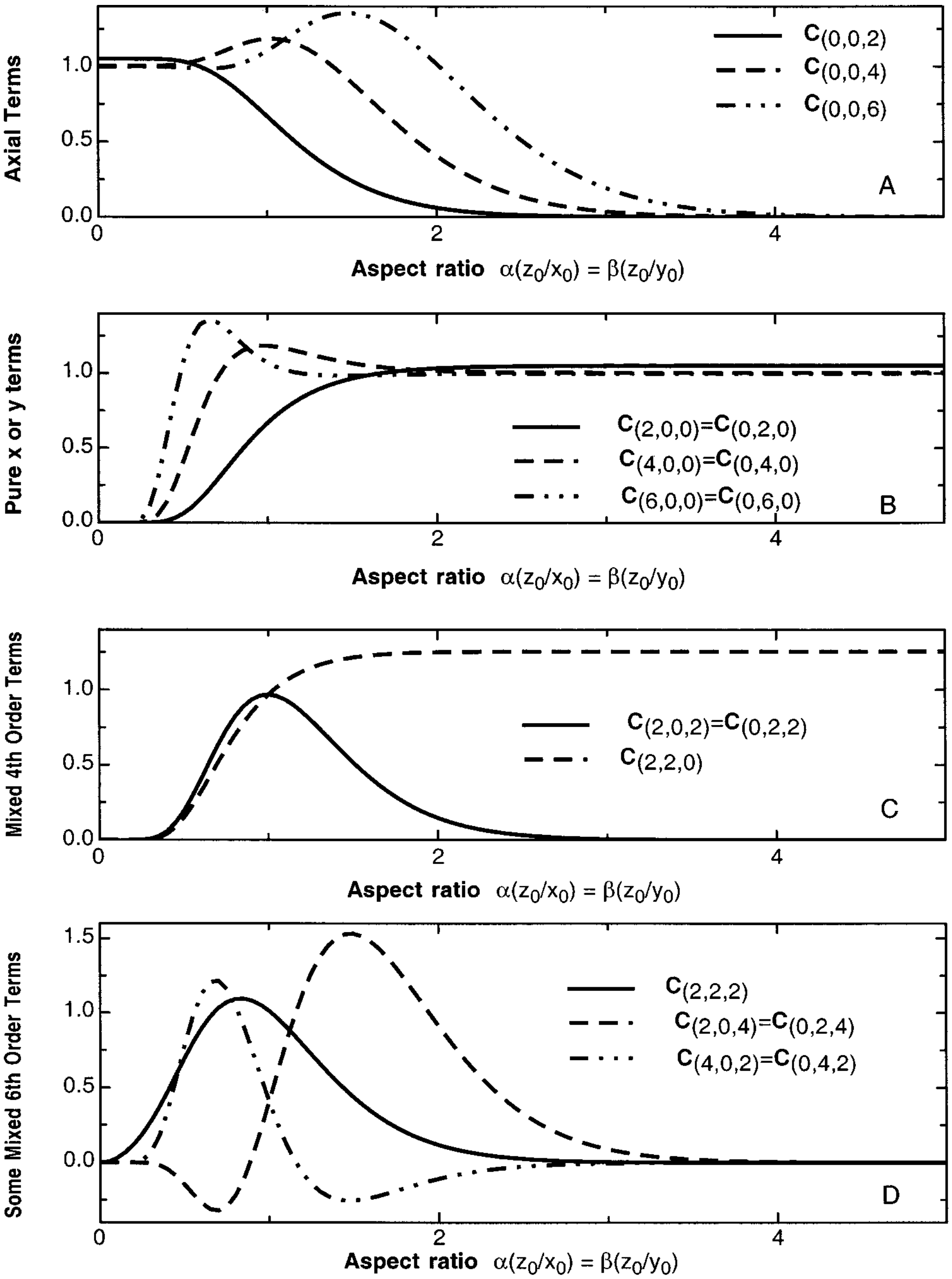

FIG. 1. Plots of the first six terms of the power series expansion of the image charge pseudopotential for a square prism as functions of the aspect ratio. (A) The pure "axial" terms—powers of $z$ only. (B) The pure "radial" terms—powers of $x$ or $y$ only. (C) The crossed "radial" terms—powers of $x$ and $y$. (D) The crossed "radial" and "axial" terms—powers of $x$ and/or $y$ and $z$.

$$T_n(\tilde{\rho},\tilde{\rho}')=\frac{I_m\left(\frac{n\pi\tilde{\rho}_<}{2}\right)}{I_m\left(\frac{n\pi}{2\alpha}\right)}\left[I_m\left(\frac{n\pi}{2\alpha}\right)K_m\left(\frac{n\pi\tilde{\rho}_<}{2}\right)-K_m\left(\frac{n\pi}{2\alpha}\right)I_m\left(\frac{n\pi\tilde{\rho}_<}{2}\right)\right], \tag{44}$$

$I_m$ and $K_m$ are modified (or "hyperbolic") Bessel functions, and the tilde indicates scaling by $z_0$ rather than by $\rho_0$. Using the identity $I_m(u)K_m'(u)-K_m(u)I_m'(u)=-1/u$, we find the surface charge on the cylindrical wall is

TABLE I. Asymptotic limits of image charge potential coefficients for Square Box.

| $\mathbf{C}_{st,2s,2u}$ <br> $\alpha=\beta$ <br> $z_0/x_0=z_0/y_0$ | $\alpha\rightarrow 0$ <br> Parallel plate | $\alpha=1$ <br> Cube | $\alpha\rightarrow 0$ <br> Square tube |
|---|---|---|---|
| $\mathbf{C}_{0,0,2}$ | 1.0518 | 0.6692 | 0 |
| $\mathbf{C}_{0,0,4}$ | 1.0045 | 1.1850 | 0 |
| $\mathbf{C}_{0,0,6}$ | 1.0005 | 1.1047 | 0 |
| $\mathbf{C}_{2,0,0}=\mathbf{C}_{0,2,0}$ | 0 | 0.6692 | 1.0518 |
| $\mathbf{C}_{4,0,0}=\mathbf{C}_{0,4,0}$ | 0 | 1.1850 | 1.0045 |
| $\mathbf{C}_{6,0,0}=\mathbf{C}_{0,6,0}$ | 0 | 1.0721 | 1.0005 |
| $\mathbf{C}_{2,0,2}=\mathbf{C}_{0,2,2}$ | 0 | 0.9690 | 0 |
| $\mathbf{C}_{2,0,4}=\mathbf{C}_{0,2,4}$ | 0 | 0.4085 | 0 |
| $\mathbf{C}_{4,0,2}=\mathbf{C}_{4,0,2}$ | 0 | 0.4085 | 0 |
| $\mathbf{C}_{2,2,0}$ | 0 | 0.9690 | 1.2557 |
| $\mathbf{C}_{2,4,0}=\mathbf{C}_{4,2,0}$ | 0 | 0.4085 | 0.269 36 |
| $\mathbf{C}_{2,2,2}$ | 0 | 1.0147 | 0 |

$$\sigma_c = \frac{-q}{2\pi\epsilon_0 z_0}\sum_{m=0}^{\infty}\sum_{n=1}^{\infty}\left\{\epsilon_m \cos[m(\phi-\phi')]\sin\left[\frac{n\pi(\tilde{z}+1)}{2}\right]\times\sin\left[\frac{n\pi(\tilde{z}'+1)}{2}\right]\frac{I_m\left(\frac{n\pi\tilde{\rho}}{2}\right)}{I_m\left(\frac{n\pi}{2\alpha}\right)}\right\}. \tag{45}$$

Squaring this double sum and integrating it to find the total radial force on the cylinder is somewhat involved. The identity

$$\int_0^{2\pi}\cos(x)\cos(mx)\cos(nx)\,dx = \begin{cases}\pi & \text{for } m=0 \text{ and } n=1\\ \pi & \text{or } m=1 \text{ and } n=0\\ \pi/2 & \text{for } m-n=\pm 1 \text{ and } n,m>0\\ 0 & \text{otherwise}\end{cases} \tag{46}$$

is useful. The radial force on the charge from Eq. (17) is

$$F_\rho = \frac{q^2}{2\pi\epsilon_0\rho_0 z_0}\sum_{m=0}^{\infty}\sum_{n=1}^{\infty}\sin^2[n\pi(\tilde{z}+1)/2]\times\frac{I_m(n\pi\tilde{\rho}/2)I_{m+1}(n\pi\tilde{\rho}/2)}{I_m(n\pi/2\alpha)I_{m+1}(n\pi/2\alpha)}. \tag{47}$$

This is the same form obtained by Xiang *et al.*[8] except that they omitted the $m=0$ terms, which are the most important.

From $F_z$ and $F_\rho$ we can find $\Phi$, except for an unknown additive constant, in two different ways

$$\Phi(\overline{\rho},\overline{z}) = -\frac{2}{q}\left\{\left[\int F_z(\overline{\rho},\overline{z})d\overline{z}\right]+\left[\int F_\rho(,\overline{\rho},0)d\overline{\rho}\right]\right\} \tag{48}$$

$$\Phi(\tilde{\rho},\tilde{z}) = -\frac{2}{q}\left\{\left[\int F_z(0,\tilde{z},)d\tilde{z}\right]+\left[\int F_\rho(\tilde{\rho},\tilde{z})d\tilde{\rho}\right]\right\}, \tag{49}$$

where care must be exercised to keep the normalizations correct. The term-by-term integration of $F_z$ is straightforward, but that of $F_\rho$ is not. The treatment of either form requires about the same amount of labor. Since we are interested in the power series expansion of $\Phi$,

$$\Phi(\overline{\rho},\overline{z}) = -\frac{q}{4\pi\epsilon_0 z_0}\sum_{m=0}^{\infty}\sum_{n=0}^{\infty}C_{m,n}(\alpha)\overline{\rho}^{2m}\overline{z}^{2n}, \tag{50}$$

we find that the second of these two forms is the more convenient. Evaluation of the integral over the radial force means integrating

$$\frac{2z_0}{n\pi}\mathfrak{R}_m\left(\frac{n\pi}{2z_0}\rho\right) \equiv \int I_m\left(\frac{n\pi}{2z_0}\rho\right)I_{m+1}\left(\frac{n\pi}{2z_0}\rho\right)d\rho, \tag{51}$$

which cannot be done in terms of well known functions. The integral can be done analytically by first expanding both Bessel functions in a power series and integrating term by term, to get

$$\mathfrak{R}_m(x) = x^{2(m+1)}\sum_{j=0}^{\infty}\frac{x^{2j}}{j+m+1}\times\sum_{k=0}^{j}\frac{1}{(j-k+m+1)!(k+m)!(j-k)!k!}. \tag{52}$$

In spite of its cumbersome appearance, $\mathfrak{R}_m(x)$ is well behaved and readily evaluated. We can now write down $\Phi(\rho,z)$ [or $\Phi(\tilde{\rho},\tilde{z})$]

$$\Phi(\rho,z) = -\frac{q}{4\pi\epsilon_0 z_0}\left[2\alpha\sum_{n=1}^{\infty}\frac{\cosh\left(2j_{0,n}\frac{z}{\rho_0}\right)}{j_{0,n}\{J_1(j_{0,n})\}^2\sinh(2\alpha j_{0,n})} + \frac{2}{\pi}\sum_{m=0}^{\infty}\sum_{n=1}^{\infty}\frac{\mathfrak{R}_m\left(\frac{n\pi}{2z_0}\rho\right)\left\{\sin\left(\frac{n\pi}{2z_0}[z_0+z]\right)\right\}^2}{nI_{m+1}\left(\frac{n\pi}{2\alpha}\right)I_m\left(\frac{n\pi}{2\alpha}\right)}\right] \tag{53}$$

or

$$\Phi(\tilde{\rho},\tilde{z}) = -\frac{q}{4\pi\epsilon_0 z_0}\left[2\alpha\sum_{n=1}^{\infty}\frac{\cosh(2j_{0,n}\alpha\tilde{z})}{j_{0,n}\{J_1(j_{0,n})\}^2\sinh(2\alpha j_{0,n})} + \frac{2}{\pi}\sum_{m=0}^{\infty}\sum_{n=1}^{\infty}\frac{\mathfrak{R}_m\left(\frac{n\pi}{2\alpha}\tilde{\rho}\right)\left\{\sin\left(\frac{n\pi}{2}[1+\tilde{z}]\right)\right\}^2}{nI_{m+1}\left(\frac{n\pi}{2\alpha}\right)I_m\left(\frac{n\pi}{2\alpha}\right)}\right]. \tag{54}$$

Expressions for the coefficients of Eq. (50) can be obtained from Eq. (53) by substituting the Taylor series expansions for $\cosh(2j_{0,n}z/\rho_0)$ and $\sin(n\pi[1+z]/2z_0)$, and rearranging terms. The first term on the right hand side of Eq. (53) [or Eq. (54)], gives us all of the pure axial terms, while the second gives all of the remaining terms excepting only the constant term, $C_{0,0}(\alpha)$.

$$C_{0,2m}(\alpha,\rho_0) = \frac{2}{(2m)!}\left(\frac{2}{\rho_0}\right)^{2m}\sum_{n=1}^{\infty}\frac{j_{0,n}^{2m}}{[J_1(j_{0,n})]^2\sinh(2j_{0,n}\alpha)} \tag{55}$$

or

$$C_{0,2m}(\alpha,z_0) = \frac{(2\alpha)^{2m+1}}{(2m)!}\sum_{n=1}^{\infty}\frac{j_{0,n}^{2m}}{[J_1(j_{0,n})]^2\sinh(2j_{0,n}\alpha)}. \tag{56}$$

For the actual numerical values in a particular instance, i.e., given $\rho_0$ and $z_0$ either expression will do. Evaluation of the purely axial terms is most readily accomplished using Eq. (56), because of its convergence properties for all $\alpha$. As expected, as $\alpha\rightarrow 0$, i.e., holding $z_0$ constant and letting $\rho_0\rightarrow\infty$, the $C_{0,2m}$'s are identical to those of the infinite parallel plate system discussed above. Use of Eq. (55) by contrast is

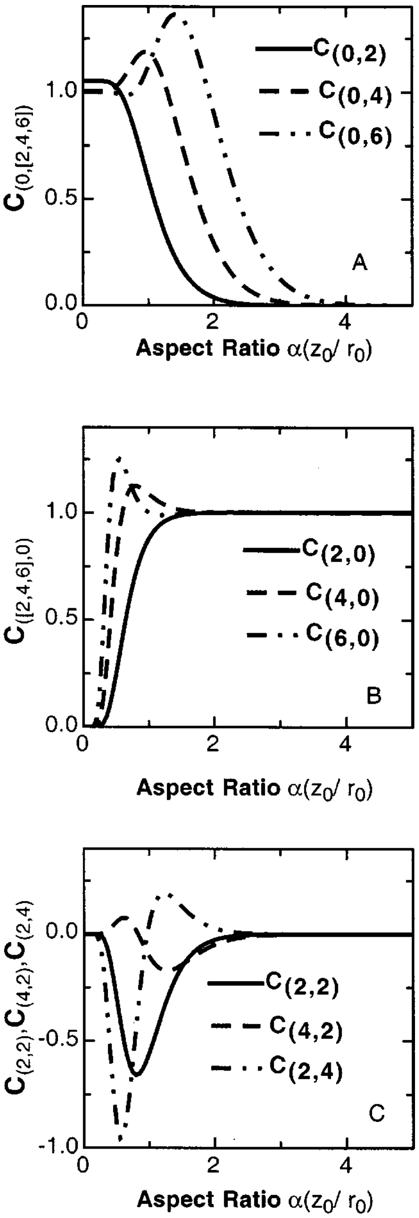

FIG. 2. Plots of the the first six terms of the power series expansion of the image charge pseudopotential for a cylindrical box as functions of the aspect ratio. (A) The pure axial terms—powers of $z$ only. (B) The pure radial terms—powers of $r$ only. (C) The crossed radial and axial terms—powers of $r$ and $z$.

equivalent to holding $\rho_0$ constant while varying $z_0$, which clearly must diverge as $\alpha\rightarrow 0$. Figure 2(A) shows plots of $C_{0,2}$, $C_{0,4}$, and $C_{0,6}$.

The coefficients for purely radial displacements follow directly from our definition of $\mathfrak{R}_m$ above; however no simple general form as in Eqs. (55) or (56) emerges. Specific forms for the low order terms, including cross terms, can be found however. It is convenient to define two variables

$$\xi_n \equiv \frac{\pi[2n-1]}{2\alpha} \tag{57}$$

and

TABLE II. Asymptotic limits of image charge coefficients for cylindrical box.

| $\mathbf{C}_{st,2s}$ | $\alpha\rightarrow 0$ Parallel plate | 4th Order exp'l. trap | $\alpha = 1$ | $\alpha\rightarrow 0$ long tube |
|---|---|---|---|---|
| $C_{0,2}$ | 1.0518 | 0.7755 | 0.5880 | 0 |
| $C_{0,4}$ | 1.0045 | 1.1669 | 1.1845 | 0 |
| $C_{0,6}$ | 1.0005 | 1.0180 | 1.1246 | 0 |
| $C_{2,0}$ | 0 | 0.7534 | 0.8792 | 1.0027[a] |
| $C_{4,0}$ | 0 | 1.1243 | 1.0884 | 1.0009 |
| $C_{6,0}$ | 0 | 1.0572 | 1.0020 | 1.0003 |
| $C_{2,2}$ | 0 | −0.9157 | −1.0309 | 0 |
| $C_{4,2}$ | 0 | −0.3470 | −0.4359 | 0 |
| $C_{2,4}$ | 0 | 0.1822 | 0.1884 | 0 |

[a] Agrees with results of Fine and Driscoll [Ref. 3, Eq. (32)].

$$\zeta_n \equiv \frac{\pi n}{2\alpha}. \tag{58}$$

Then

$$C_{2,0} = \frac{1}{\alpha}\sum_{n=1}^{\infty}\frac{\xi_n}{I_0(\xi_n)I_1(\xi_n)}, \tag{59}$$

$$C_{4,0} = \frac{1}{16\alpha}\sum_{n=1}^{\infty}\frac{\xi_n^3(3I_2(\xi_n)+I_0\xi_n)}{I_0(\xi_n)I_1(\xi_n)I_2(\xi_n)}, \tag{60}$$

$$C_{6,0} = \frac{1}{576\alpha}\sum_{n=1}^{\infty}\xi_n^5\left\{\frac{10}{I_0(\xi_n)I_1(\xi_n)} + \frac{5}{I_1(\xi_n)I_2(\xi_n)} + \frac{1}{I_2(\xi_n)I_3(\xi_n)}\right\}, \tag{61}$$

$$C_{2,2} = \frac{\alpha}{2}\sum_{n=1}^{\infty}\frac{(-1)^n\zeta_n^3}{I_0(\zeta_n)I_1(\zeta_n)}, \tag{62}$$

$$C_{2,4} = -\frac{\alpha^3}{24}\sum_{n=1}^{\infty}\frac{(-1)^n\zeta_n^5}{I_0(\zeta_n)I_1(\zeta_n)}, \tag{63}$$

and

$$C_{4,2} = \frac{\alpha}{32}\sum_{n=1}^{\infty}\frac{(-1)^n\zeta_n^5[3I_2(\zeta_n)+I_0(\zeta_n)]}{I_0(\zeta_n)I_1(\zeta_n)I_2(\zeta_n)}. \tag{64}$$

The limiting values listed in Table II are again in line with our generic discussion above. These coefficient terms are shown plotted in Figs. 2(B) and 2(C). The experimental data shown below were gathered with a cylindrical ion trap where $z_0 = 1.66$ cm and $r_0 = 2.00$ cm, so $\alpha = 0.8314$ and $D_0 = 0.02357$.

## IV. EXAMPLES FROM PENNING TRAPS

As we stated in the introduction, a major motivation for undertaking this study was to quantify the image effects on ion motion in Penning ion traps. A general treatment of the Penning trap lies well outside the scope of this article. However, a brief introduction will serve to illustrate how image charge can affect experimental observation. Much more detailed treatments can be found in References 3, 16, and 17.

Ions of a single charge sign are stored in a Penning trap through the combined effects of static electric and magnetic fields. For simplicity, we take the magnetic field to be uniform and parallel to the $z$ axis

$$\mathbf{B}=B_0\hat{\mathbf{z}}. \tag{65}$$

The magnetic field provides radial confinement of ions, while the electric field provides axial confinement. The electric field itself is produced by biassing the trap electrodes with appropriate voltages. In addition to the radial confinement by the magnetic field, there is always some radial electric field whose force is directed outwards. The result is an $\mathbf{E}\times\mathbf{B}$ drift in the $\Theta$ direction. For an ion of charge $q$ and mass $M$ in a circular orbit of radius $r_\pm$, one can show[16] that its orbital frequency is given by

$$\omega_\pm=\frac{\Omega}{2}\left\{1\pm\sqrt{1-\frac{4}{M\Omega^2}\left[\frac{F(r)}{r}\right]_{r=r_\pm}}\right\}, \tag{66}$$

where $\Omega=qB/M$ is the cyclotron frequency and $F(r)$ is the radial force. The "+" sign in Eq. (66) is the high frequency motion that we call the ion cyclotron resonance frequency while the "−" sign refers to the generally much lower $\mathbf{E}\times\mathbf{B}$ drift frequency. This latter motion is generally known as the "magnetron" or "diocotron" frequency, depending on whether the dominant source of the radial force is due to the trapping fields or image charge, respectively. It is easy to show from Eq. (66) that

$$\omega_+=\Omega-\omega_-. \tag{67}$$

Since $\Omega\sim\omega_+\gg\omega_-$, $\omega_-$ reduces to the simple approximation

$$\omega_-\approx\frac{E(r)/r}{B}. \tag{68}$$

Thus, to first order, $\omega_-$ is independent of both ion mass and charge. Further, it is clear from Eq. (67) that if $\omega_-$ is understood, the ICR frequencies are also described. From the linearity inherent in the theory of electric and magnetic fields, $E(r)$ may be evaluated as a simple sum over all of its source terms. This in turn allows us to describe the various contributions to the drift frequency in the approximation of Eq. (68)

$$\omega_-\approx\omega_-(\text{Trap fields})+\omega_-(\text{Image Field})+\omega_-(\text{Other}). \tag{69}$$

## A. The cubical ICR cell

At this point we can ask the question: Under normal operating conditions, in a standard instrument, how large are image charge effects likely to be? For the sake of concreteness, we consider a cubical ICR cell of dimension $x_0=y_0=z_0=D_0$, and whose z axis is aligned parallel to a uniform magnetic field $\mathbf{B}=B_0\hat{z}$. From Eqs. (35), (36), (68), and (69)

$$\omega_-(\text{Image Field})\approx\frac{q}{M\Omega r}\left\{-\frac{1}{2}\frac{\partial\Phi_{\text{image}}(r,\theta,z)}{\partial r}\right\}_{r=r_{\text{cm}}} \tag{70}$$

or keeping only the linear terms of the pseudopotential

$$\omega_-(\text{Image Field})\approx\frac{1}{B}\left\{\frac{qN}{4\pi\epsilon_0 D_0^3}\right\}C_{2,0,0}. \tag{71}$$

Using the value of $C_{2,0,0}$ from Table I and taking $D_0=4$ cm, the shift in the observed magnetron frequency due to image charges, $f_{m,\text{image}}$, is

$$f_{-,\text{image}}\approx 1.92(10)^{-5}N/B\,\text{Hz}, \tag{72}$$

where $N$ is the number of elementary charges and the magnetic field $B$ is in Teslas. This is a small effect, but can be readily detected in some cases.

## B. Estimating effects due to axial extension

Up to here we have considered the effects of image charge on compact, i.e., point-like ion clouds. With certain restrictions and simplifications, approximations for extended ion clouds can be found. This development is necessary in order to couple the forgoing developments to the experimental observations presented below. When many ions are simultaneously stored in a Penning trap, they rapidly approach a thermal equilibrium state through ion–ion collisions.[16,17] This equilibrium can be characterized by ion number, total canonical angular momentum and energy (or temperature).[16,17] (To simplify the discussion, we will restrict ourselves to ion clouds of a single charge to mass ratio.) An ion cloud at thermal equilibrium rotates rigidly about its own axis[3] with a frequency $\omega_r$ that is determined by trapping fields and its own space charge. (Image charge plays only a secondary role here.)

For cases of practical interest in mass spectroscopy, we may further assume that the ion cloud's radius, $r_p$ and length $2z_p$ are small compared to the trap's radius and length, respectively. Under these conditions, we find experimentally that a resonance excitation near either $\omega_+$ or $\omega_-$ causes the entire ion cloud to orbit the trap's center like a single body. We interpret this motion as a translating equilibrium state.[16] It is not unusual to observe these "modes" for tens of thousands to millions of periods. In the language of nonneutral plasma physics these are the undamped upper and lower diocotron modes.[3] Experimentally these modes *are* damped, but the damping is due primarily to ion-neutral collisions and to nonlinearities in the trapping field (see discussion below). Further, no experimental evidence has emerged for $k_z\neq 0$ associated with these modes. That is, no drift modes where ions at differing axial positions orbit with different amplitudes or frequencies have been reported to our knowledge. Thus we feel justified in treating the excited ion cloud as a rigid body that moves in a mean field.

In yet another simplification, we adopt the "cold fluid model,"[16–19] where the ion cloud is described approximately by a spheroid of uniform charge density.[20] A cold ion cloud can be characterized by three parameters, its half-length $z_p$, its radius $r_p$, and its charge density $n_0$ or total charge $N$. (Another model that treats the cloud as a uniform rod of finite length has been employed elsewhere.[21] A similar model was also used and explained in detail by Fine and Driscoll.[7]) With the above restrictions, we can average the radial forces due to nonlinear terms along the length of the cloud. The average values of $z^2$ and $z^4$ over the spheroidal cloud are

$$\langle z^2\rangle = 0.5 z_p^2 \tag{73}$$

and

$$\langle z^4\rangle = \sqrt{0.5} z_p^4 . \tag{74}$$

These are the values we use later to describe magnetron frequencies and their shifts when nonlinear effects become observable.

### C. The "fourth order" cylindrical ICR cell

In order to investigate the role that trapping fields play in ICR mass spectrometry, we constructed a cylindrical Penning trap with an aspect ratio ($\alpha = z_0/r_0$) of 0.8314. The electrostatic potential of the trap near the center is

$$\Phi_{\text{Trap}}(r,z) \approx V_T\left[\frac{0.936}{r_0^2}\left(\frac{1}{2}r^2 - z^2\right) - \frac{0.227}{r_0^6}\times\left(\frac{5}{16}r^6 - \frac{45}{8}r^4z^2 + \frac{15}{2}r^2z^4 - z^6\right)\right], \tag{75}$$

where $V_T$ is the applied trapping potential and $r_0 = 2$ cm is the trap radius. By design, the fourth order terms in the trapping potential are missing. The coefficient of the quadratic term is our best experimental determination; and to within our ability to measure, the fourth order term is zero. The coefficient of the sixth order term is the result of a computation. The image charge pseudopotential for the trap is found by evaluating the results of Section E. Eqs. (56)–(62) for $\alpha = 0.8314$, and assuming $N$ ions of charge $q$

$$\Phi_{\text{image}}(r,z) \approx -\frac{qN}{4\pi\epsilon_0 r_0}\left[\frac{0.753r^2}{r_0^2} + \frac{0.776z^2}{r_0^2} + \frac{1.124r^4}{r_0^4} - \frac{0.916r^2z^2}{r_0^4} + \frac{1.167z^4}{r_0^4}\right]. \tag{76}$$

With the help of Eq. (68) we may write

$$\omega_- \approx \frac{q}{M\Omega r}\left\{-\frac{\partial\Phi_{\text{Trap}}(r,z)}{\partial r} - \frac{1}{2}\frac{\partial\Phi_{\text{image}}(r,z)}{\partial r}\right]. \tag{77}$$

Substitution from Eqs. (75) and (76) and making use for the mean values found above gives

$$f_- \approx \frac{V_T}{B}(372.42 - 0.001\,058 r_-^4 + 0.006\,35 r_-^2 z_p^2 - 0.005\,99 z_p^4) + \frac{N}{B}(21.57 + 0.161 r_-^2 - 0.0328 z_p^2)\,\text{Hz}. \tag{78}$$

Equation (78) is written in "convenience" units, i. e., $r_-$ and $z_p$ are in millimeters; $N$ is in millions; while $V_T$ and $B$ remain in SI units.

Figure 3 shows the experimental time evolution of magnetron motion for two large electron clouds stored in this trap. Here $V_T = 30.00$ V and $B = 7.0469$ T. The electron cloud was produced by electron bombardment of background gas and required 40 s with a 100 eV, 10 nA beam. We estimate that the background pressure was $\approx 2(10)^{-9}$ Torr. Since each ionization event will produce two electrons, the cloud had approximately $10^7$ electrons.[22] The zero of time was taken at the point that the ionization electron beam was switched off.

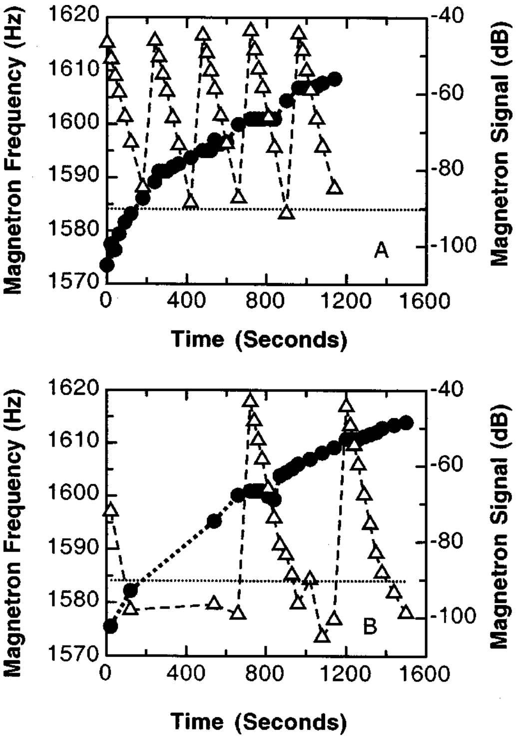

FIG. 3. Evolution of electron magnetron signal in 4th order ICR cell. ● measured magnetron frequency, △ measured magnetron signal amplitude, connecting lines are for clarity. Periodic increases of magnetron signal are due to a weak external dipole excitation. Empty trap magnetron frequency.

In both cases we note that magnetron motion appeared spontaneously during the production of the electron cloud. Currently, we have no explanation for the appearance of magnetron motion during the production of electron clouds, but we do regularly observe the effect. Subsequent excitation of magnetron motion was produced by a resonant chirp. The signal data indicate that no particles were lost during the course of the measurement and that the two electron clouds were essentially identical. We also note that the damping of the magnetron motion is very similar in all cases. Other experiments showed that at low background pressure, the damping rate of magnetron motion is roughly proportional to electron number, not neutral density. This may be an additional manifestation of anharmonic effects that couple center of mass motion to internal motion of individual particles.[23] In comparing both the signal and frequency data of Figs. 3(a) and 3(b) we see that the repeated magnetron excitations had little or no perceptible effects on the gross features of the time evolution. Figure 3(b) illustrates another mysterious feature; namely, the magnetron motion never completely disappeared, although its amplitude became small. This may be the result of low amplitude noise in the system or may point to something more fundamental.

Turning our attention now to the frequency data, we see a number of interesting effects. (The dotted line in Figs. 3(a) and 3(b) is the expected empty trap magnetron frequency.) First, we note that the gross features of the frequency evolu-

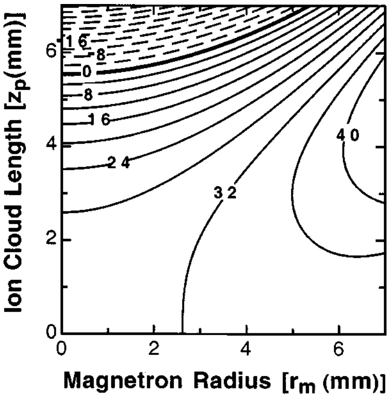

FIG. 4. Expected magnetron frequency shift in an experimental Penning trap as a function of ion cloud length and magnetron (or cyclotron) radius in cylindrical box trap with $\alpha = 0.8314$, $r_0 = 2$ cm, $B = 7.0469$ T, and $10^7$ elementary charges. Dashed contours denote values less than 0.

tion are unaffected by the magnetron excitations. The initial magnetron frequencies are nearly identical, as is the rate of frequency evolution. Second, we see that with magnetron excitation, the frequency jumps up by a small amount and then stays nearly constant during the major portion of the damping, after which it starts to rise again.

The general trends of the frequency evolution can be explained by radial transport. That is, the electron cloud has some initial length determined by the trapping potential and the cloud's parameters of radius and ion number. Electron-neutral collisions or other sources of torque drive radial transport. As the cloud expands radially, it shortens axially. The effects of ion cloud length and magnetron amplitude are illustrated in Fig. 4. Figure 4 is a contour plot of Eq. (78) in which we have taken $N = 10$ million and set the zero to the empty trap frequency. If the ion cloud had an initial half length, $z_p \approx 6$ mm, the magnetron frequency would shift about 10 Hz below the empty trap value. As it shortens due to radial transport, the magnetron frequency grows. Magnetron excitation also causes the frequency to increase. During the damping of the magnetron motion, the competing effects of radial expansion and loss of magnetron amplitude keep the frequency nearly constant. We do not, however, have sufficient data to show whether the very constant frequency during damping observed here is more than just coincidence.

Figure 4 itself is illustrative, not quantitative. The specific contours, their separation and shape are sensitive to the exact value of $N$. Currently, we have no good way to get more than a factor of two estimate of this number. Interestingly, when we try to fit $z_p$ to the time evolution of the frequency data within this uncertainty of $N$, we find that $z_p$ decreases approximately linearly with time with a rate of $1-6(10)^{-3}$ mm/s depending on the assumed value on $N$. We also find that the magnetron excitations in Fig. 3 were 1–1.5 mm. The data are inadequate to make any more precise assignments.

### D. Implications for ICR mass spectrometry

In chemical applications of ICR mass spectrometry, ions of various mass to charge ratios are simultaneously stored in the trap. After allowing for thermalization, all of the ions are excited by a dipole rf field transverse to **B** whose frequency is swept through the resonant ICR frequencies. Ions at each different mass remain clustered together and gyrate about the center of the trap at their respective ICR frequencies. This motion induces image currents on ''receiver'' antennas and the ions are detected. Typically, these signals are digitized and passed through a fast Fourier transform to produce a power spectrum. The power spectrum is converted to a mass spectrum with the help of a variant of Eq. (66). Both the excitation and detection antennas are segments of the trap electrodes that lie parallel to the magnetic field.

Mass spectrometers are evaluated by several parameters, including mass resolution, dynamic range, sensitivity, mass precision and accuracy, reproducibility, and ''throughput.'' (This latter term refers to how many measurements and remeasurements can be made per unit time.) As with any type of spectroscopy, ultimate performance in any one of these areas generally occurs at the expense of others. A highly skilled operator can generally find conditions that give satisfactory results for a particular problem. In the identification and characterization of large biomolecules, the tremendous mass resolution as well as its high throughput make ICR an attractive tool. The trick is to accurately relate the observed frequencies to masses.

According to Eq. (67) the difference between the observed ICR frequency, $\omega_+$ and the actual cyclotron frequency, $\Omega$ is just the drift frequency.[24] Thus, amplitude and ion abundance dependent frequency shifts can be largely interpreted in terms of their effects on the drift frequency. As we have shown, image charge gives rise to both linear and nonlinear terms in the radial electric fields. Further, when the trapping fields also contain nonlinearities, they must be included with the image charge effects in the interpretation of data.

## V. CONCLUSIONS

We have shown how the forces on charges that arise from charge distributions that they induce may be cast in the form of a potential that we call the ''image charge pseudopotential.'' The ''pseudopotential'' concept allows us to readily compute the forces on a charged particle (or compact group of charges) located interior to a variety of electrode geometries, e.g., in ion traps. By using the pseudopotential formalism we can bring these effects into our calculations on an equal footing with other forces. Thus, estimates of frequency shifts and perturbations of orbits in Penning traps can be made in rather straightforward ways. Further, our formalism allows us to see an essential unity that applies to all cases. Namely, when the image charge pseudopotential is expressed in the standard form of Eq. (22), the coefficients of the various powers of the coordinates all vary between $\approx \pm 1$. Interestingly, the most complicated fields are those associated with length to width ratios ($\alpha$'s) between 1 and 2, which is just the range where most trap designs fall.

## ACKNOWLEDGMENTS

The research described in this article was performed at the W. R. Wiley Environmental Molecular Sciences Laboratory, a national scientific user facility sponsored by the Department of Energy's Office of Biological and Environmental Research and located at Pacific Northwest National Laboratory. Pacific Northwest National Laboratory is operated for the U.S. Department of Energy by Battelle under Contract No. DE-AC06-76RLO 1830. This work is supported in part by the U.S. Department of Energy Office of Basic Energy Sciences, Chemical Sciences Division.

[1] T. J. Francl, M. G. Sherman, R. L. Hunter, M. J. Locke, W. D. Bowers, and R. T. McIver, Int. J. Mass Spectrom. Ion Processes **54**, 188 (1983).

[2] K. R. Spangenberg, *Vacuum Tubes* (McGraw-Hill, New York, 1948), p. 482f.

[3] R. C. Davidson, *Physics of Non Neutral Plasmas* (Addison-Wesley, Redwood City, CA, 1990).

[4] S. V. Jefferts, T. Heavener, P. Hayes, and G. H. Dunn, Rev. Sci. Instrum. **64**, 737 (1993).

[5] B. L. Maschhoff and J. P. Cowin, J. Chem. Phys. **101**, 8138 (1994).

[6] R. S. Van Dyck, P. B. Schwinberg, and H. G. Dehmelt, Phys. Rev. Lett. **38**, 310 (1977).

[7] K. S. Fine and C. F. Driscoll, Phys. Plasmas **5**, 601 (1998).

[8] X. Xiang, P. B. Grosshans, and A. G. Marshall, Int. J. Mass Spectrom. Ion Processes **125**, 33 (1993).

[9] E. C. Beaty, J. Appl. Phys. **61**, 2118 (1987).

[10] G. Gabrielse, L. Haarsma, and S. L. Rolston, Int. J. Mass Spectrom. Ion Processes **88**, 319 (1989).

[11] G. Gabrielse and F. C. Mc MacIntosh, Int. J. Mass Spectrom. Ion Processes **57**, 1 (1984).

[12] W. R. Smythe, *Static and Dynamic Electricity*, 3rd ed. (McGraw-Hill, New York, 1968), Chap. 3 [esp. Eq. 3.08 (2)].

[13] L. S. Brown and G. Gabrielse, Rev. Mod. Phys. **58**, 233 (1986).

[14] R. Mittleman, H. Dehmelt, and S. Kim, Phys. Rev. Lett. **75**, 2839 (1995).

[15] J. D. Jackson, *Classical Electrodynamics*, 2nd ed. (Wiley, New York, 1975), p. 54f.

[16] A. J. Peurrung, R. T. Kouzes, and S. E. Barlow, Int. J. Mass Spectrom. Ion Processes **157/158**, 39 (1996).

[17] D. H. E. Dubin and T. M. O'Neil, Rev. Mod. Phys. **71**, 87 (1999).

[18] S. A. Prasad and T. M. O'Neil, Phys. Fluids **22**, 278 (1979).

[19] J. J. Bollinger, D. J. Heinzen, F. L. Moore, W. M. Itano, D. J. Wineland, and D. H. E. Dubin, Phys. Rev. A **48**, 525 (1993).

[20] The careful reader will recognize a certain inconsistency here. As $T \to 0$, so too must the bounce frequency in an actual nonneutral plasma (as opposed to an ion cloud whose length $z_p \ll \lambda_D$, the Debye shielding length). Experimentally we can justify the assumption of an axially rigid plasma (assuming a uniform magnetic field) because for both magnetron and cyclotron motions no axial waves have ever been reported for finite geometries. (In the language of wave mechanics, $k_z = 0$.) This observation can be explained for the magnetron mode as being due to $f_m \ll f_z$, but fails in the opposite limit of the cyclotron mode where $f_z \ll f_{\mathrm{ICR}}$. Even the imposition of highly anharmonic trapping potentials, such as in the standard ICR cell, apparently does not give rise to $k_z \neq 0$. It may well be the case that something more profound is at work here.

[21] M. V. Gorshkov, A. G. Marshall, and E. N. Nikolaev, J. Am. Soc. Mass Spectrom. **4**, 855 (1993).

[22] S. E. Barlow and M. D. Tinkle, Rapid Commun. Mass Spectrom. **13**, 390 (1999).

[23] B. P. Cluggish and C. F. Driscoll, Phys. Rev. Lett. **74**, 4213 (1995).

[24] The proof of this statement lies beyond the work here and may be generalized somewhat more. When the magnetron and cyclotron amplitudes are identical (a zero canonical angular momentum state), the ion cloud or individual particles pass through the point $r = 0$ during each cyclotron orbit. One can show that in this state too, $\Omega = \omega_+ + \omega_-$.